

Crack tip shielding and size effect related to parallel edge cracks under uniaxial tensile loading

*Original*

Crack tip shielding and size effect related to parallel edge cracks under uniaxial tensile loading / Ferrian, F., Cornetti, P., Sapora, A., Talebi, H., Ayatollahi, M.R.. - In: INTERNATIONAL JOURNAL OF FRACTURE. - ISSN 0376-9429. - 245:3(2024), pp. 223-233. [10.1007/s10704-023-00756-1]

*Availability:*

This version is available at: 11583/2988491 since: 2024-05-11T10:13:39Z

*Publisher:*

Springer

*Published*

DOI:10.1007/s10704-023-00756-1

*Terms of use:*

This article is made available under terms and conditions as specified in the corresponding bibliographic description in the repository

*Publisher copyright*

(Article begins on next page)



RESEARCH

# Crack tip shielding and size effect related to parallel edge cracks under uniaxial tensile loading

Francesco Ferrian · Pietro Cornetti · Alberto Sapora · Hossein Talebi · Majid R. Ayatollahi

Received: 18 May 2023 / Accepted: 8 December 2023 / Published online: 22 February 2024  
© The Author(s) 2024

**Abstract** The present work aims at investigating crack shielding and size effect related to a cracked slab under tensile loading. For this purpose, experimental tests are carried out on PMMA cracked samples. Three different geometries are taken into account, presenting one, two or three parallel edge cracks, and assuming their distance equal to their initial length. Results are interpreted through the coupled stress and energy criterion of Finite Fracture Mechanics (FFM). The approach is implemented numerically, and parametric finite element analyses are carried out to evaluate the normal stress field and the stress intensity factor for each configuration. It is found that asymmetric crack propagation has to be preferred according to the energy balance. The matching between FFM failure predictions and experimental data reveals to be satisfactory.

**Keywords** FFM · Crack shielding · Size effect · PMMA · Asymmetric propagation · Energy balance

## 1 Introduction

The strength of mechanical components is strongly affected by the presence of cracks, which give rise to local stress concentrations and can result in the brittle collapse of the structure. The interaction between cracks leads to enhancing/shielding phenomena, which have great influence on the failure mechanism and cannot be neglected (Mahadevan and Shi 2001; Tan and Chen 2015; Shu et al. 2017). Focusing on crack shielding, for instance, due to the proximity of the cracks, the “effective crack-driving force” actually experienced at their tips is locally reduced (Ritchie 1988). The driving force for crack growth is generally described by a field-characterizing parameter, the stress intensity factor (SIF), which characterizes the stress and strain fields in the singular region close to the crack tip. Accordingly, the SIF at the tips of the shielded cracks is lower, and hence the failure load is higher.

Aim of this study is to analyse the crack shielding and failure size effect regarding a tensile slab presenting one, two or three parallel edge cracks. For this purpose, two experimental campaigns are conducted by tensile testing polymethyl methacrylate (PMMA) cracked plates. The initial crack length and their

---

F. Ferrian · P. Cornetti · A. Sapora (✉)  
Department of Structural, Geotechnical and Building Engineering, Politecnico di Torino, Corso Duca degli Abruzzi 24, 10129 Turin, Italy  
e-mail: alberto.sapora@polito.it

H. Talebi · M. R. Ayatollahi  
Fatigue and Fracture Research Laboratory, Center of Excellence in Experimental Solid Mechanics and Dynamics, School of Mechanical Engineering, Iran University of Science and Technology, Tehran, Iran

distance are both set equal to 0.1 times the sample width  $w$  for reasons of practicality. Size effects are highlighted by varying  $w$  in the slab presenting two interacting cracks. Note that different catastrophic failures are related to the interaction between parallel edge cracks. To cite but a few, let us mention those related to aero-engine turbines (Martín-Meizoso et al. 1995), actuator piston rods (Rütti and Wentzel 1998) and pressure vessels (Parker 1999).

The theoretical framework is developed by means of the Finite Fracture Mechanics (FFM) approach. FFM is a coupled fracture criterion which allows to provide strength predictions based on the simultaneous fulfilment of a stress condition and the energy balance. Originally proposed in the static framework (Leguillon 2002), (Cornetti et al. 2006), it was recently applied in the fatigue limit regime (Sapora et al. 2020), (Liu et al. 2020). The approach rests on the assumption of finite crack advance in contrast to Linear Elastic Fracture Mechanics (LEFM), which assumes crack growth to develop continuously. Note that LEFM fails to deal with very short cracks, according to which the SIF tends to vanish and the approach provides an infinite failure load. On the other hand, FFM is able to overcome this drawback catching the transition from a strength- to a toughness-governed regime, as the crack length varies (Cornetti et al. 2006), (Cornetti and Sapora 2019). Similar arguments hold when dealing with ligament size effect in largely cracked tensile structures (Sapora et al. 2023). As regards the notch size effect, FFM has been applied to brittle failure in presence of circular holes (Doitrand and Sapora 2020), (Doitrand and Leguillon 2021), (Leite et al. 2021), square holes (Doitrand et al. 2021) and spherical or spheroidal voids (Chao Correias et al. 2021), (Ferrian et al. 2023). A computational coupled implementation was proposed in (Wegert et al. 2022) to estimate the strength of a plate with centre crack, circle, diamond, and hexagon perforations of different sizes. Finally, let us mention the study carried out in (Doitrand et al. 2017) to assess the influence of a crack on the initiation and propagation of other cracks in woven composites.

In order to implement FFM, the knowledge of the stress field and SIF expressions is required. This task is here accomplished numerically by parametric Finite Element Analysis (FEA) through ANSYS® code. Note that different works focused on the

evaluation of the SIF for parallel edge cracks configurations, exploiting analytical approaches (Freese 1976), (Civelek and Erdogan 1982), numerical simulations (Jiang et al. 1990), (Jiang et al. 1992), (Gope et al. 2014), (Bisht et al. 2015), (Mariggiò et al. 2023) and experimental methods (Farahmand and Raftopoulos 1981), (Raftopoulos and Farahmand 1982).

The paper is organized as follows. The experimental campaign on PMMA cracked samples and related results are presented in Sect. 2, whereas the FFM criterion and its numerical implementation are introduced in Sect. 3. Crack shielding and failure size effect are described in detail. Section 4 presents the comparison with experimental data, whereas Sect. 5 is voted to conclusions.

## 2 Experimental investigation

In order to analyse the crack shielding and failure size effect, uniaxial tensile tests are carried out on cracked plates made of PMMA. Samples are machined by laser cutting PMMA sheets and sharpening the crack tips through a fresh razor blade. The sheet thickness  $t$  is equal to 5 mm to ensure plane strain conditions, according to the relationship  $t \geq 2.5 l_{ch}$  (Taylor 2007), where  $l_{ch} = (K_{Ic}/\sigma_c)^2$  is the well-known Irwin's length and it is generally comprised between 0.2 and 1 mm for PMMA (Seweryn 1994), (Taylor 2007). Here,  $K_{Ic}$  denotes the plain fracture toughness and  $\sigma_c$  refers to the tensile strength.

Two different experimental campaigns are performed at a constant displacement rate of 0.5 mm/min. The first one is related to the crack shielding investigation. The samples are weakened by the presence of one, two or three edge cracks perpendicular to the loading direction (Figs. 1a, b, c). The width  $w$  of the samples is set equal to 30 mm, whereas the parameters  $a_0$  and  $d$  representing the initial crack length and the distance between cracks, respectively, are both taken equal to 3 mm (hence,  $a_0/w = d/w = 0.1$ ), to point out the crack shielding phenomenon. Furthermore, the length  $L$  is considered equal to 150 mm, five times higher than  $w$ . Four samples are considered for each configuration, for a total of 12 tested geometries. From the images of the broken samples (Fig. 2a), it is possible to state that the crack propagation is asymmetric (involving

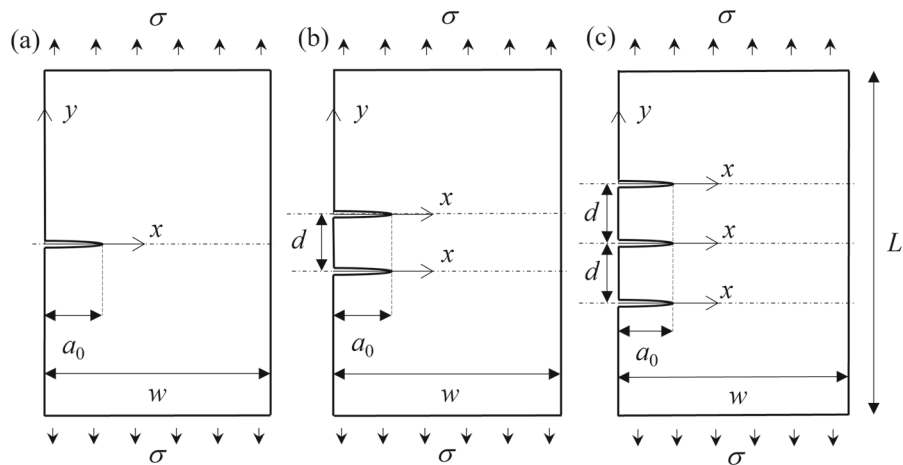


**Fig. 1** Tensile slab presenting one **a**, two **b** or three **c** edge cracks

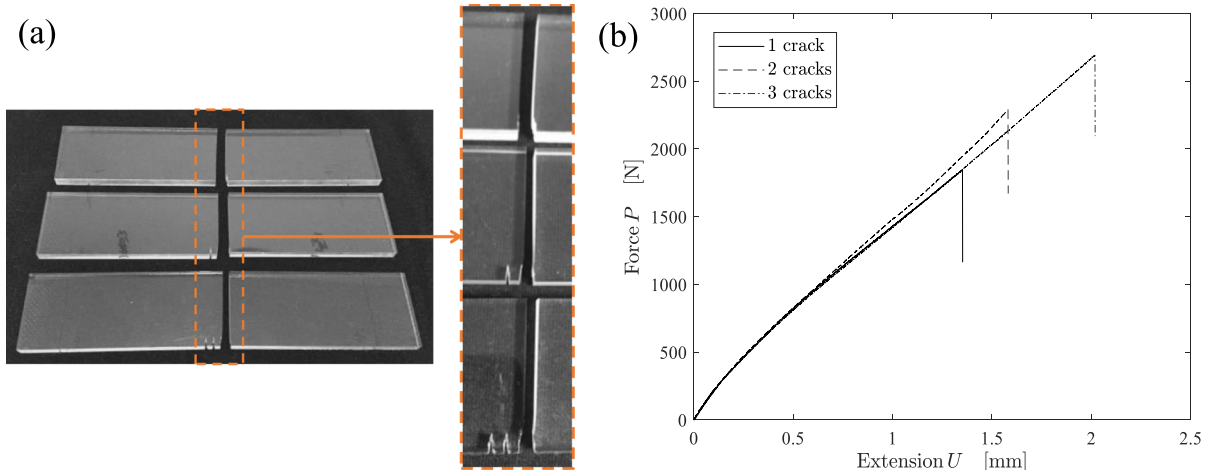


**Fig. 2** **a** Cracked configurations analysed in the study and **b** related force-extension curves

always one external crack tip) in the configurations with two and three parallel cracks. Moreover, the failure is of brittle character and plastic deformation is negligible around the crack tip, as evident from the force-extension curves represented in Fig. 2b.

The second one is devoted to analyse the failure size effect. Referring to the configuration presenting two cracks and keeping fixed  $a_0/w=d/w=0.1$ , two additional geometries are considered by varying the size as  $w=10\text{ mm}$  ( $a_0=d=1\text{ mm}$ ,  $L=50\text{ mm}$ ) and  $w=50\text{ mm}$  ( $a_0=d=5\text{ mm}$ ,  $L=250\text{ mm}$ ), see Fig. 3a. Again, during these tests, the failure is of brittle character (Fig. 3b), showing the increase of the

failure load  $P_f=\sigma_f(w \times t)$  at which the crack starts to propagate as the size  $w$  increases.

For all tested cracked geometries, the recorded failure loads  $P_f$  are reported in Table 1: the scatter of recorded values, always lower than 3.5%, proves the significant test repeatability.

As concerns the crack propagation, as previously mentioned, an asymmetric one was observed for all the analysed configurations (Figs. 2 and 3). It is important to note that this outcome may be influenced by sample machining and micro-imperfections in the material. In order to minimize the uncertainty related to this aspects, crack lengths were measured carefully

before the test. Moreover, to ensure the accuracy and repeatability of the experimental results, each test was repeated four times. As presented in Table 1, the scatter of the experimental results is very small, indicating that sample preparation and testing were performed with very good accuracy.

The mechanical properties of PMMA are presented in Table 2. The ultimate tensile strength  $\sigma_c$  as well as Young’s modulus  $E$  and Poisson’s ratio  $\nu$  were estimated following ASTM D638-14 standard code. Instead, the fracture toughness  $K_{Ic}$  was evaluated in order to minimize the standard deviation between the experimental data and avg-FFM failure

estimations for the former experimental campaign (see Sect. 4). Accordingly,  $K_{Ic}=1.52 \text{ MPa}\sqrt{\text{m}}$  and  $l_{ch}=0.51 \text{ mm}$ . These values fall within the typical ranges measured for PMMA (Taylor 2007), (Sapora et al. 2015), (Cicero et al. 2018).

### 3 Finite Fracture Mechanics (FFM)

The theoretical framework is developed by means of the FFM approach. Accordingly, finite crack propagation occurs when a stress condition and the energy balance are simultaneously fulfilled. The stress

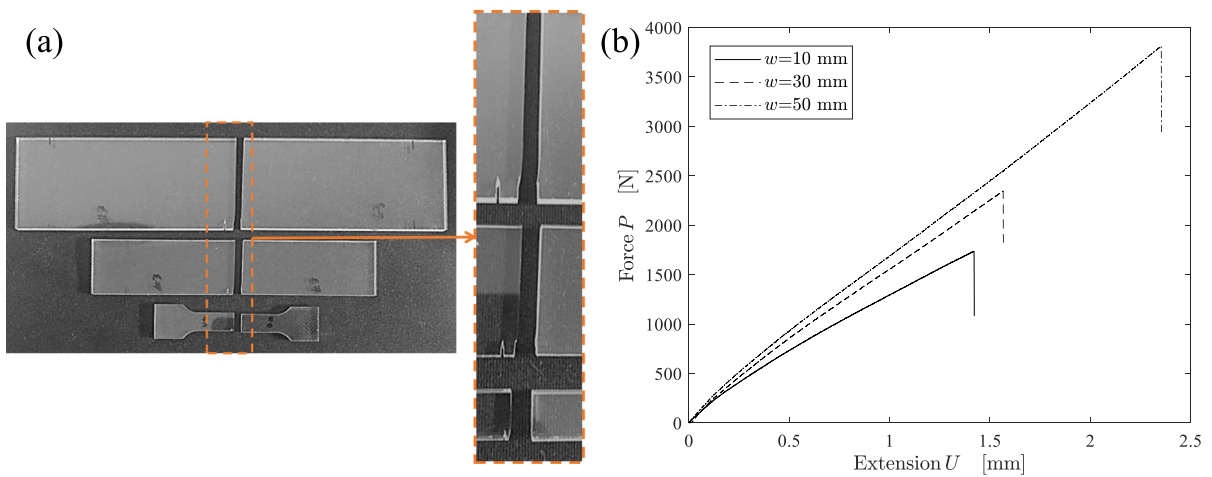


**Fig. 3** Failure size effect: **a** Tested geometries and **b** corresponding force-extension curves

**Table 1** Tensile tests on PMMA cracked samples: characteristic dimensions and recorded failure loads

Number of cracks	$w$ (mm)	$P_f$ (N)				$P_{f,avg}$ (N)
1	30	1858	1847	1852	1865	$1856 \pm 6.7$
	10	1688	1735	1654	1719	$1699 \pm 31$
2	30	2346	2367	2292	2414	$2355 \pm 44$
	50	3814	3842	3761	3911	$3832 \pm 54$
3	30	2507	2547	2692	2452	$2550 \pm 89$

**Table 2** PMMA mechanical properties obtained experimentally except from the value of  $K_{Ic}$  that is fitted on avg-FFM failure estimations

$\sigma_c$ (MPa)	$K_{Ic}$ (MPa $\sqrt{\text{m}}$ )	$E$ (GPa)	$\nu$
$67.32 \pm 0.65$	1.52	$2.90 \pm 0.11$	$0.38 \pm 0.017$

requirement, considering the approach proposed by (Leguillon 2002), imposes that the normal stress  $\sigma_y$  over a finite distance  $l$  must be larger than the ultimate tensile strength  $\sigma_c$  of the material. On the other hand, the energy balance ensures that the integration of the strain energy  $G$  over a finite crack increment  $l$  must exceed  $G_c l$ , where  $G_c$  is the material fracture energy. This last condition can be recast exploiting Irwin's relationship, thus introducing the SIF  $K_I = \sqrt{(GE')}$  and fracture toughness  $K_{Ic} = \sqrt{(G_c E')}$ ,  $E'$  being Young's modulus of the material under plane strain conditions. Particularizing the FFM formulation to the (positive) geometries analysed in this study and to the Cartesian frame of reference  $(x, y)$  (Fig. 1), yields:

$$\begin{cases} \sigma_y(x = a_0 + l) = \sigma_c \\ \int_{a_0}^{a_0+l} K_I^2(a') da' = K_{Ic}^2 l \end{cases} \quad (1)$$

The approach can be also developed considering an average stress condition (Cornetti et al. 2006), (Carpinteri et al. 2008), requiring that the average normal stress  $\sigma_y$  over a distance  $l$  must exceed  $\sigma_c$ . Accordingly, the avg-FFM approach writes:

$$\begin{cases} \int_{a_0}^{a_0+l} \sigma_y(x) dx = \sigma_c l \\ \int_{a_0}^{a_0+l} K_I^2(a') da' = K_{Ic}^2 l \end{cases} \quad (2)$$

In Sect. 3.3 it will be shown that, in critical conditions ( $\sigma = \sigma_f$ ), the two unknowns of FFM systems (1) or (2) are represented by the remote failure stress  $\sigma_f$ , implicitly embedded in the stress field and the SIF functions, and the critical crack increment  $l_c$ . This latter quantity will reveal to be a structural parameter, since dependent on both material and geometric characteristics.

### 3.1 Finite element analysis (FEA)

The stress field and the SIF functions related to the geometries under investigation, necessary for the FFM implementation as shown above, can be expressed as:

$$\sigma_y = \sigma S(x/w) \quad (3)$$

$$K_I = \sigma \sqrt{\pi a} F_I(a/w) \quad (4)$$

where  $S(x/w)$  and  $F_I(a/w)$  are the shape functions related to the stress field and SIF, respectively.

In this work, for each geometry,  $S(x/w)$  and  $F_I(a/w)$  are determined through parametric FEAs by ANSYS® code. Quadratic elements, with 6 nodes and characterized by a reduced integration solution scheme are implemented under plane strain conditions. To obtain accurate results, following a convergence analysis, the mesh is refined within a circle of radius  $0.5a_0$  centered at the crack tip (Fig. 4): therein, the minimum dimension of the elements is set equal to  $0.01a_0$ .

### 3.2 Symmetric vs asymmetric crack propagation

In critical conditions, considering an isotropic and homogeneous material, a crack is expected to initiate from the crack tip along the  $x$ -axis for the single edge cracked configuration (Fig. 1a). Instead, taking into account the other two geometries, two different cases need to be analysed: (i) Symmetric and (ii) Asymmetric crack initiation. More in detail, referring to the double cracked configuration (Fig. 1b), cracks could initiate simultaneously from the two crack tips (once  $d/w=0.1$  is fixed) or asymmetrically from only one crack tip (once  $d/w=a_0/w=0.1$  are fixed), Fig. 5b. Comparing the maximum values of  $K_I$ , i.e.  $K_{I_{max}}$ , the most critical scenario results to be the asymmetric one. Indeed, the corresponding SIF is nearly 8% higher considering  $a/w=0.11$ . This result is in agreement with the experimental observations reported in Sect. 2 (Figs. 2a and 3a).

Analogously, for the third configuration (Fig. 1c), comparing  $K_{I_{max}}$  related to all possible scenarios, the most critical one results to be the asymmetric crack initiation from one of the two external cracks (Fig. 5c). This result is once again in agreement with the experimental evidence (Fig. 2a). Indeed, considering  $a/w=0.11$ , the corresponding SIF is 18% higher than  $K_{I_{max}}$  related to symmetric initiation from the three crack tips. Taking into account the propagation from the central crack or the simultaneous initiation from two cracks, the value of  $K_{I_{max}}$  related to the most critical scenario is 13% and 9% higher, respectively. Thus, henceforth only the asymmetric crack initiation from one of the two outer cracks will be analysed.

The trend of the SIF shape functions  $F_I(a/w)$ , related to the three analysed cracked configurations, is shown in Fig. 6 as the ratio  $a/w$  varies between 0.1

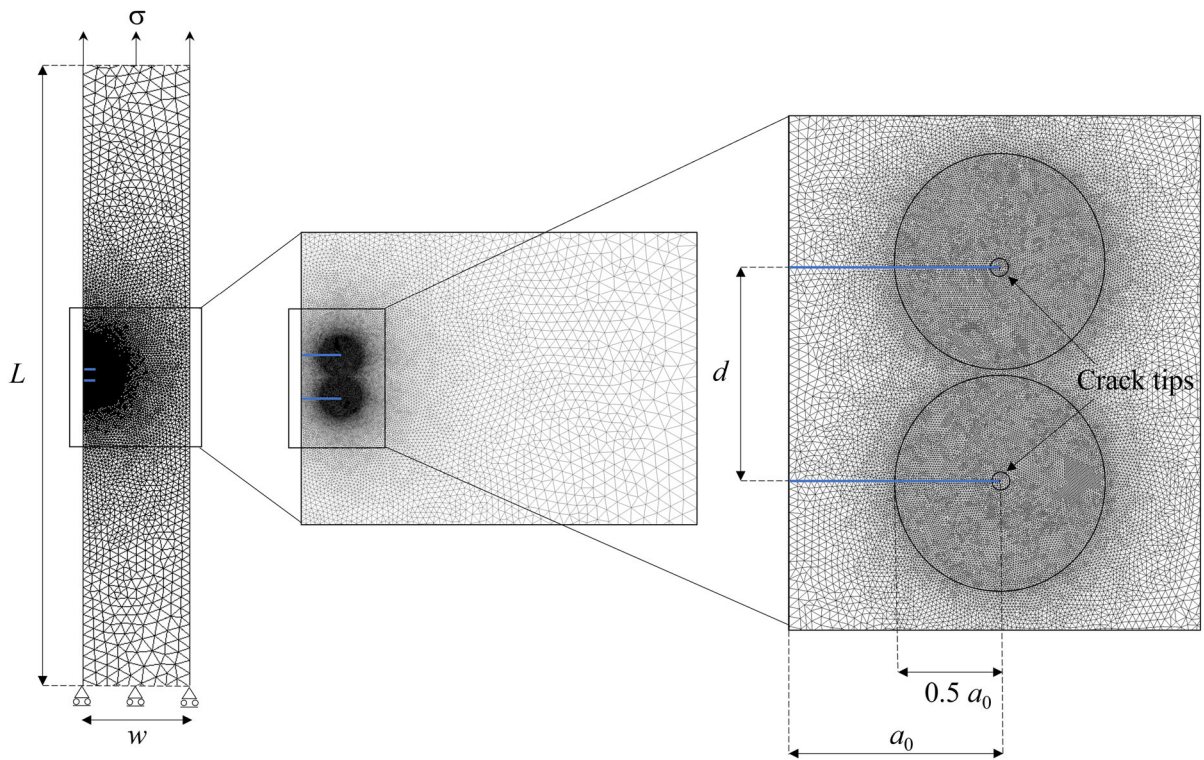


**Fig. 4** Finite element model for the geometry presenting two interacting cracks. The model refers to symmetric crack propagation. It is assumed that  $a_0=d=0.1 w$ , coherently with experimental data

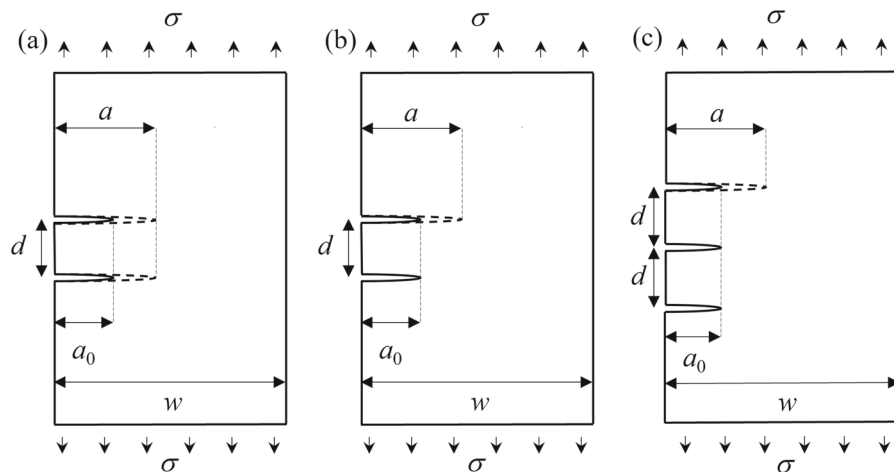


**Fig. 5** Symmetric **a** vs. asymmetric **b** crack propagation for the tensile plate presenting two interacting cracks; **c** most critical scenario regarding the triple cracked configuration

and 0.5. As regards asymmetric propagation, significant differences are present as long  $a/w < 0.2$ , i.e., when  $a < 2a_0$ . For the geometry with two interacting cracks (Fig. 1b), both symmetric and asymmetric crack initiation cases are reported according to our

simulations and to the analytical approximating expression proposed by Jiang et al. (1990), Jiang et al. (1992). The deviation from the values hereby computed in this work is less than 3 and 1% in the symmetric and asymmetric cases, respectively.

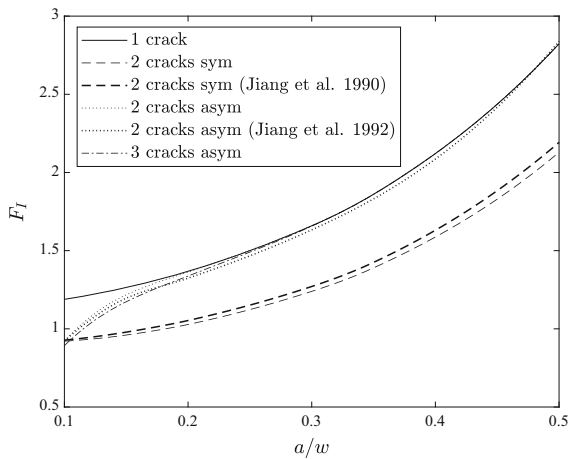


**Fig. 6** Shape functions  $F_I$  related to single, double or triple edge cracked geometries

Finally, it is worth observing that, for the configuration presenting two cracks and for the two outer cracks in the triple cracked geometry,  $K_{II}$  is not zero, as it can be easily argued since these cracks do not lie on a symmetry axis. However, it can be easily checked that mode mixity angle is really small. Hence, throughout our investigation, we have disregarded the mode II contribution. Note that this hypothesis was assumed also in (Jiang et al. 1990) and is confirmed experimentally by our tests, characterized by an almost collinear crack growth (Figs. 2 and 3).

### 3.3 FFM implementation

FFM can now be implemented, in critical conditions ( $\sigma = \sigma_f$ ), for each of the three configurations analysed. Introducing the stress field (3) and the SIF (4) into Eq. (1), yields:

$$\begin{cases} \frac{\sigma_f}{\sigma_c} = \frac{1}{S[(a_0 + l_c)/w]} \\ \frac{\sigma_f}{\sigma_c} = \sqrt{\frac{l_{ch}}{\pi} \frac{l_c}{\int_{a_0}^{a_0+l_c} a' F_I^2(a'/w) da'}} \end{cases} \quad (5)$$

FFM failure estimations are obtained by equalling the right-hand sides of system (5) to get  $l_c$  through the solution of an implicit equation. This value is then introduced into one of the two equations in (5) to get the corresponding dimensionless failure stress.

On the other hand, as concerns avg-FFM, introducing Eqs. (3) and (4) into Eq. (2), yields:

$$\begin{cases} \frac{\sigma_f}{\sigma_c} = \frac{l_c}{\int_{a_0}^{a_0+l_c} S(x/w) dx} \\ \frac{\sigma_f}{\sigma_c} = \sqrt{\frac{l_{ch}}{\pi} \frac{l_c}{\int_{a_0}^{a_0+l_c} a' F_I^2(a'/w) da'}} \end{cases} \quad (6)$$

which can be solved analogously to Eq. (5).

Strength estimations according to FFM are reported in Fig. 7a. As evident, the normalized failure stress  $\sigma_f / \sigma_c$  decreases as the dimensionless width  $w/l_{ch}$  increases catching the typical failure size effect. For sufficiently large sizes, coupled approaches revert to LEFM and the single edge cracked plate results to be the most critical configuration. The deviation in terms of failure stress from the other two geometries tends to 30% (two cracks) and 33% (three cracks) as  $w/l_{ch} \rightarrow \infty$ . This behaviour can be justified by the crack shielding phenomenon that characterizes the configurations with more than one crack.

It is worthwhile to underline that, for vanishing  $w/l_{ch}$ , the normalized failure stress  $\sigma_f / \sigma_c$  converges to 0.9 according to avg-FFM, coherently with the initial fixed ratio  $a/w=0.1$  (Fig. 1). On the other hand, FFM provides a dimensionless failure load  $\sigma_f / \sigma_c \approx 1.1$ . As observed in other works (Sapora et al. 2023), this is a questionable FFM trend as the crack advance approaches the ligament width.

In Fig. 7b the critical crack advancement  $l_c/l_{ch}$  is plotted as a function of the normalized width  $w/l_{ch}$ , thus revealing a structural parameter and not just a material one, as it happens for Theory of Critical Distance (TCD) approaches (Taylor 2007). Avg-FFM provides higher  $l_c/l_{ch}$  values with respect to FFM, as already established in past studies (e.g. (Ferrian et al. 2023)). Indeed, for all cracked configurations analysed, the failure mechanism is governed by the fracture toughness for large sizes and the stress condition only provides the critical crack advancement. It converges to  $1/(2\pi)$  or  $2/\pi$  taking into account FFM (Eq. (5)) or avg-FFM (Eq. (6)), respectively: in the former case, the value coincides with the distance according to TCD point method, in the latter case it matches the estimation by TCD line method (Taylor 2007), (Cicero et al. 2012), (Ayatollahi et al. 2016).

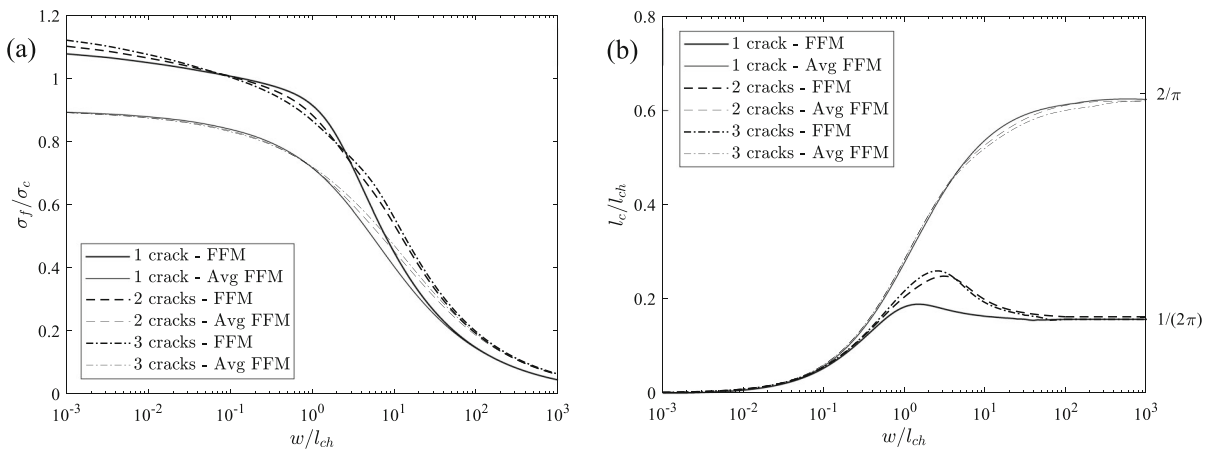


**Fig. 7** Strength estimations  $\sigma_f/\sigma_c$  **a** and critical crack advancements  $l_c/l_{ch}$  **b** provided by FFM (thick curves) and avg-FFM (thin curves) for single, double and triple cracked configurations

**4 FFM estimations vs experimental results**

FFM failure predictions are now compared with experimental data presented in Sect. 2. As concerns the first experimental campaign related to crack shielding, results are reported in Table 3.

Indeed, taking into account avg-FFM predictions, the maximum deviation from the average value of the experimental failure load is around 3% for the configurations with one and three cracks, whereas is lower than 1.5% for the plate with two interacting cracks. It should be underlined, as observed preliminarily in Sect. 2, that the value of fracture toughness for PMMA was fitted on avg-FFM predictions. Also FFM results are accurate and deviations always keep below 6.5%. Similar arguments hold for LEFM, which provides the highest predictions.

On the other hand, as concerns the second experimental campaign, results are depicted in Fig. 8: the difference between FFM predictions according to symmetric and asymmetric crack propagation decreases as the size increases, both converging to LEFM estimations. It is worth emphasizing that the

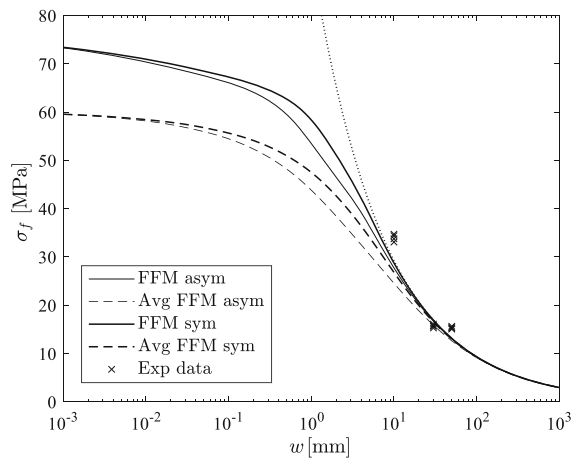


**Fig. 8** Size effect on the plate containing two interacting cracks: comparison between experimental data and theoretical FFM results. The dotted line represents LEFM predictions

ability to discriminate between symmetrical and asymmetrical crack propagation is a strength point of the present FFM approach. In fact, lying on the assumption of an infinitesimal crack growth, LEFM provides the same crack onset load value if one or

**Table 3** Failure stress related to tensile PMMA cracked samples ( $w=30$  mm): experimental data, FFM and LEFM predictions

N° cracks	$\sigma_{f,avg}$ (MPa)	$\sigma_f$ , FFM (MPa)	Deviation (%)	$\sigma_f$ , avg FFM (MPa)	Deviation (%)	$\sigma_f$ , LEFM (MPa)	Deviation (%)
1	12.4	13.1	+5.6	12.8	+3.2	13.2	+6.5
2	15.7	16.7	+6.4	15.9	+1.2	17.1	+9.0
3	17.0	17.3	+1.8	16.5	-2.9	17.6	+3.5

both cracks propagate in the configuration presenting two interacting cracks (and one or both outer cracks in the three-edge crack configuration). Note that TCD shows the same drawback as LEFM does, since TCD depends only on the stress field before crack growth. Finally, note that avg-FFM always reveals the most conservative approach, as typically observed in the field of brittle failure of cracked/notched structures (Sapora et al. 2023), (Ferrian et al. 2023).

Basically, the curves related to the asymmetric case are the most critical ones confirming experimental observations (Fig. 2a) and numerical results (Sect. 3.2). Taking into account avg-FFM predictions obtained for asymmetric crack initiation, the maximum deviation from the average value of the experimental failure stress is equal to 26.6% for the first configuration ( $w=10$  mm) and 17.5% for the third one ( $w=50$  mm). Instead, considering FFM, the maximum deviation decreases to 18% and 14.8% for the first and the third geometry, respectively.

## 5 Conclusions

In this study, three different tensile configurations were analysed presenting one, two or three parallel edge cracks. Both the length and the distance between cracks were set equal to 0.1 times the width of geometry. Experimental tests were carried out on PMMA cracked samples and the results were compared with theoretical failure estimations obtained by means of the coupled FFM approach, which requires the simultaneous fulfilment of a stress condition and the energy balance. The stress field and SIF functions -necessary for FFM implementation- were obtained through parametric FEAs. It was shown that, due to crack shielding, propagation always occurred asymmetrically and increasing the number of cracks increased the strength of the structure. Indeed, due to the proximity of the shielded cracks, the lower the SIFs at their tips, the higher the failure load. Furthermore, also the failure stress size effect was analysed varying the sample dimension for the configuration presenting two interacting cracks. Unfortunately, the range investigated experimentally was limited and it was not possible to fully investigate the range where LEFM predictions are meaningless ( $w < 1-2$  mm, Fig. 8). This drawback could be overcome testing materials which are less

brittle than PMMA. In this regard, let us mention that the coupled FFM approach was recently applied to catch the size effect related to single cracked geometries (Cornetti et al. 2006; Baldassari et al. 2023), validating the results by considering experimental data on concrete and rock samples present in the Literature.

**Author contributions** H.T. carried out the experiments. F.F. carried out the numerical simulations and prepared all figures. F.F. and A.S. wrote the main text. P.C., A.S., M.A. supervised all work and reviewed the manuscript.

**Funding** Open access funding provided by Politecnico di Torino within the CRUI-CARE Agreement.

## Declarations

**Competing interests** The authors declare no competing interests.

**Open Access** This article is licensed under a Creative Commons Attribution 4.0 International License, which permits use, sharing, adaptation, distribution and reproduction in any medium or format, as long as you give appropriate credit to the original author(s) and the source, provide a link to the Creative Commons licence, and indicate if changes were made. The images or other third party material in this article are included in the article's Creative Commons licence, unless indicated otherwise in a credit line to the material. If material is not included in the article's Creative Commons licence and your intended use is not permitted by statutory regulation or exceeds the permitted use, you will need to obtain permission directly from the copyright holder. To view a copy of this licence, visit <http://creativecommons.org/licenses/by/4.0/>.

## References

- Ayatollahi MR, Torabi AR, Rahimi AS (2016) Brittle fracture assessment of engineering components in the presence of notches: a review. *Fatigue Fract Eng Mater Struct* 39:267–291. <https://doi.org/10.1111/ffe.12379>
- Baldassari M, Monaco A, Sapora A, Cornetti P (2023) Size effect on flexural strength of notched and un-notched concrete and rock specimens by Finite Fracture Mechanics. *Theor Appl Fract Mech* 125:103787. <https://doi.org/10.1016/j.tafmec.2023.103787>
- Bisht N, Gope PC, Panwar K (2015) Influence of crack offset distance on the interaction of multiple cracks on the same side in a rectangular plate. *Frat Ed Integrità Strutt* 9:1–12. <https://doi.org/10.3221/IGF-ESIS.32.01>
- Carpinteri A, Cornetti P, Pugno N et al (2008) A finite fracture mechanics approach to structures with sharp V-notches.

- Eng Fract Mech 75:1736–1752. <https://doi.org/10.1016/j.engfracmech.2007.04.010>
- Chao Correas A, Corrado M, Sapora A, Cornetti P (2021) Size-effect on the apparent tensile strength of brittle materials with spherical cavities. *Theor Appl Fract Mech* 116:103120. <https://doi.org/10.1016/j.tafmec.2021.103120>
- Cicero S, Madrazo V, Carrascal IA (2012) Analysis of notch effect in PMMA using the theory of critical distances. *Eng Fract Mech* 86:56–72. <https://doi.org/10.1016/j.engfracmech.2012.02.015>
- Cicero S, Torabi AR, Madrazo V, Azizi P (2018) Prediction of fracture loads in PMMA U-notched specimens using the equivalent material concept and the theory of critical distances combined criterion. *Fatigue Fract Eng Mater Struct* 41:688–699. <https://doi.org/10.1111/ffe.12728>
- Civelek MB, Erdogan F (1982) Crack problems for a rectangular plate and an infinite strip. *Int J Fract* 19:139–159. <https://doi.org/10.1007/BF00016570>
- Cornetti P, Sapora A (2019) Penny-shaped cracks by finite fracture mechanics. *Int J Fract* 219:153–159. <https://doi.org/10.1007/s10704-019-00383-9>
- Cornetti P, Pugno N, Carpinteri A, Taylor D (2006) Finite fracture mechanics: a coupled stress and energy failure criterion. *Eng Fract Mech* 73:2021–2033. <https://doi.org/10.1016/j.engfracmech.2006.03.010>
- Doitrand A, Leguillon D (2021) Asymptotic analysis of pore crack initiation near a free edge. *Theor Appl Fract Mech* 116:103125. <https://doi.org/10.1016/j.tafmec.2021.103125>
- Doitrand A, Sapora A (2020) Nonlinear implementation of finite fracture mechanics: a case study on notched Brazilian disk samples. *Int J Non Linear Mech* 119:103245. <https://doi.org/10.1016/j.ijnonlinmec.2019.103245>
- Doitrand A, Fagiano C, Hild F et al (2017) Mesoscale analysis of damage growth in woven composites. *Compos Part A Appl Sci Manuf* 96:77–88. <https://doi.org/10.1016/j.compositesa.2017.02.018>
- Doitrand A, Cornetti P, Sapora A, Estevez R (2021) Experimental and theoretical characterization of mixed mode brittle failure from square holes. *Int J Fract* 228:33–43. <https://doi.org/10.1007/s10704-020-00512-9>
- Farahmand B, Raftopoulos DD (1981) Determination of the stress intensity factor for parallel and symmetric edge cracks under pure bending. *Eng Fract Mech* 14:439–458. [https://doi.org/10.1016/0013-7944\(81\)90012-6](https://doi.org/10.1016/0013-7944(81)90012-6)
- Ferrian F, Chao Correas A, Cornetti P, Sapora A (2023) Size effects on spheroidal voids by finite fracture mechanics and application to corrosion pits. *Fatigue Fract Eng Mater Struct* 46:875–885. <https://doi.org/10.1111/ffe.13902>
- Freese CE (1976) Periodic edge cracks of unequal length in a semi-infinite tensile sheet. *Int J Fract* 12:125–134. <https://doi.org/10.1007/BF00036015>
- Gope PC, Bisht N, Singh VK (2014) Influence of crack offset distance on interaction of multiple collinear and offset edge cracks in a rectangular plate. *Theor Appl Fract Mech* 70:19–29. <https://doi.org/10.1016/j.tafmec.2014.04.001>
- Jiang ZD, Zeghloul A, Bezine G, Petit J (1990) Stress intensity factors of parallel cracks in a finite width sheet. *Eng Fract Mech* 35:1073–1079. [https://doi.org/10.1016/0013-7944\(90\)90135-4](https://doi.org/10.1016/0013-7944(90)90135-4)
- Jiang ZD, Petit J, Bezine G (1992) An investigation of stress intensity factors for two unequal parallel cracks in a finite width plate. *Eng Fract Mech* 42:129–138. [https://doi.org/10.1016/0013-7944\(92\)90284-L](https://doi.org/10.1016/0013-7944(92)90284-L)
- Leguillon D (2002) Strength or toughness? A criterion for crack onset at a notch. *Eur J Mech A/Solids* 21:61–72. [https://doi.org/10.1016/S0997-7538\(01\)01184-6](https://doi.org/10.1016/S0997-7538(01)01184-6)
- Leite A, Mantič V, París F (2021) Crack onset in stretched open hole PMMA plates considering linear and non-linear elastic behaviours. *Theor Appl Fract Mech* 114:102931. <https://doi.org/10.1016/j.tafmec.2021.102931>
- Liu Y, Deng C, Gong B (2020) Discussion on equivalence of the theory of critical distances and the coupled stress and energy criterion for fatigue limit prediction of notched specimens. *Int J Fatigue* 131:105326. <https://doi.org/10.1016/j.ijfatigue.2019.105326>
- Mahadevan S, Shi P (2001) Corrosion fatigue reliability of aging aircraft structures. *Prog Struct Eng Mater* 3:188–197. <https://doi.org/10.1002/pse.77>
- Marigliò G, Ventura G, Corrado M (2023) A probabilistic FEM approach for the structural design of glass components. *Eng Fract Mech* 282:109157. <https://doi.org/10.1016/j.engfracmech.2023.109157>
- Martín-Meizoso A, Martínez-Esnaola JM, Fuentes-Pérez M (1995) Interactive effect of multiple crack growth on fatigue. *Theor Appl Fract Mech* 23:219–233. [https://doi.org/10.1016/0167-8442\(95\)00024-9](https://doi.org/10.1016/0167-8442(95)00024-9)
- Parker AP (1999) Stability of arrays of multiple edge cracks. *Eng Fract Mech* 62:577–591. [https://doi.org/10.1016/S0013-7944\(98\)00110-6](https://doi.org/10.1016/S0013-7944(98)00110-6)
- Raftopoulos DD, Farahmand B (1982) An investigation of stress intensity factors for plates with equal and unequal parallel edge cracks. *Int J Fract* 20:223–239. <https://doi.org/10.1007/BF01140337>
- Ritchie RO (1988) Mechanisms of fatigue crack propagation in metals, ceramics and composites: role of crack tip shielding. *Mater Sci Eng A* 103:15–28. [https://doi.org/10.1016/0025-5416\(88\)90547-2](https://doi.org/10.1016/0025-5416(88)90547-2)
- Rütti TF, Wentzel EJ (1998) Investigation of failed actuator piston rods. *Eng Fail Anal* 5:91–98. [https://doi.org/10.1016/S1350-6307\(98\)00005-3](https://doi.org/10.1016/S1350-6307(98)00005-3)
- Sapora A, Cornetti P, Carpinteri A, Firrao D (2015) An improved finite fracture mechanics approach to blunt v-notch brittle fracture mechanics: experimental verification on ceramic, metallic, and plastic materials. *Theor Appl Fract Mech* 78:20–24. <https://doi.org/10.1016/j.tafmec.2015.04.004>
- Sapora A, Cornetti P, Campagnolo A, Meneghetti G (2020) Fatigue limit: crack and notch sensitivity by finite fracture mechanics. *Theor Appl Fract Mech* 105:102407. <https://doi.org/10.1016/j.tafmec.2019.102407>
- Sapora A, Ferrian F, Cornetti P et al (2023) Ligament size effect in largely cracked tensile structures. *Theor Appl Fract Mech* 125:103871. <https://doi.org/10.1016/j.tafmec.2023.103871>
- Seweryn A (1994) Brittle fracture criterion for structures with sharp notches. *Eng Fract Mech* 47:673–681. [https://doi.org/10.1016/0013-7944\(94\)90158-9](https://doi.org/10.1016/0013-7944(94)90158-9)
- Shu Y, Li Y, Duan M, Yang F (2017) An X-FEM approach for simulation of 3-D multiple fatigue cracks and application to double surface crack problems. *Int J Mech Sci*

130:331–349. <https://doi.org/10.1016/j.ijmecsci.2017.06.007>

Tan JT, Chen BK (2015) Prediction of fatigue life in aluminium alloy (AA7050-T7451) structures in the presence of multiple artificial short cracks. *Theor Appl Fract Mech* 78:1–7. <https://doi.org/10.1016/j.tafmec.2015.06.001>

Taylor D (2007) *The theory of critical distances*. Elsevier, London

Wegert ZJ, Challis VJ, Grotowski JF, Roberts AP (2022) Explaining the competition between strength and toughness in perforated plates using computational finite fracture mechanics. *Theor Appl Fract Mech* 122:103615. <https://doi.org/10.1016/j.tafmec.2022.103615>

**Publisher's Note** Springer Nature remains neutral with regard to jurisdictional claims in published maps and institutional affiliations.

Springer Nature or its licensor (e.g. a society or other partner) holds exclusive rights to this article under a publishing agreement with the author(s) or other rightsholder(s); author self-archiving of the accepted manuscript version of this article is solely governed by the terms of such publishing agreement and applicable law.